CERTAIN ANALYTICAL ASPECTS OF AC-DC POWER SYSTEM WITH FACTS CONTROLLERS IN SMART GRID

Abstract

This abstract presents a comprehensive overview of the AC-DC load flow solutions, a critical components and studies related to power systems for modern electrical grids. The integration of renewable energy sources (RES) and developments in transmission networks based on high voltages in the form of high-voltage direct current (HVDC) transmission systems have necessitated the development of advanced load flow techniques that can accurately model and results optimal power flows in hybrid AC-DC systems. AC-DC load flow analysis follows a numerical algorithm to calculate steady-state power flow across mixed AC and HVDC networks. Unlike traditional AC load flow, this method considers additional parameters, such as HVDC converter characteristics, control strategies, and interconnection constraints. By effectively incorporating these factors, the algorithm enables better representation of power flow dynamics and facilitates the integration of RES and large-scale HVDC transmission. The detailed representation of various components in AC and HVDC is crucial to capturing the system's behavior accurately. Special attention is given to HVDC converters, which can significantly impact power flow and controls line power flow and bus voltage. The abstract concludes by highlighting the importance of AC-DC load flow analysis in ensuring the reliable and secure operation of contemporary power systems. As renewable energy sources and HVDC transmission continue to gain prominence, understanding and implementing accurate load flow methods are essential for achieving a sustainable and resilient energy future.

Authors

Chintalapudi V Suresh
Professor
Department of Electrical and Electronics Engineering
Vasireddy Venkatadri Institute of Technology, Nambur, Guntur, Andhra Pradesh, India.
venkatasuresh3@vvit.net

B. Sreenivasa Raju
Associate Professor
Department of Electrical and Electronics Engineering
Vasireddy Venkatadri Institute of Technology, Nambur, Guntur, Andhra Pradesh, India.
eee.raju@gmail.com

Keywords: AC-DC load flow, power system analysis, HVDC transmission, renewable energy integration, power flow optimization.

I. INTRODUCTION

Due to the developments in societal needs, the power industry has witnessed significant transformations, driven by the increasing adoption of RES and the need for long-distance electricity transmission. This shift has led to the integration of HVDC transmission into traditional alternating current (AC) power systems, giving rise to hybrid AC-DC power grids. However, the efficient and reliable operation of such hybrid systems necessitates a deeper understanding of power flow interactions between AC and DC components. The load flow analysis has long been a fundamental technique used to analyze power systems, ensuring that the demand and supply of electricity are balanced while maintaining stable voltage levels. Historically focused on AC networks, traditional load flow methods may prove inadequate when it comes to addressing the unique characteristics and complexities introduced by HVDC transmission. The AC-DC load flow analysis emerges as a crucial tool to address these challenges and cater to the evolving power system landscape. Unlike conventional AC load flow, the AC-DC load flow analysis extends its scope to encompass both AC and HVDC components, considering the characteristics of HVDC converters, power control strategies, commutation processes, and transmission constraints.

In this, we discuss the key components of the AC-DC load flow analysis, including: **AC and HVDC Network Modeling**: The detailed representation of AC and HVDC system components, is crucial to capturing the system's behavior accurately. Special attention is given to HVDC converters, which can significantly impact power flow because of their capacity to regulate the transmission of power and voltage. **Hybrid AC-DC Power Flow Equations**: The load flow equations are modified to include HVDC power control equations and additional constraints imposed by the HVDC transmission system. These modified equations provide a comprehensive understanding of the interactions between the AC and DC components, enabling accurate power flow calculations. **Control Strategies and Stability Considerations**: HVDC systems employ various control strategies to regulate power flow and maintain system stability. The abstract explores the impact of these control mechanisms on overall power flow and system performance, including stability analysis. **Optimization Techniques**: With the increasing complexity of modern power systems, optimization techniques play a vital role in enhancing system efficiency and reliability. The abstract discusses various refinement techniques such as the Newton-Raphson and Gauss-Seidel algorithms, employed for efficiently resolving the AC-DC load flow challenge.

The main objectives of the AC-DC load flow analysis are twofold: accurate representation and efficient optimization. Firstly, it aims to accurately model the behavior of HVDC systems within the context of a broader power network, ensuring that the interactions between AC and DC components are well understood and appropriately accounted for. Secondly, the analysis seeks to optimize power flow paths and maximize the utilization of the transmission infrastructure, minimizing losses and enhancing overall energy efficiency. Renewable energy integration plays a significant role in the evolution of modern power systems. The intermittent nature of renewable resources necessitates dynamic power flow management to ensure smooth integration and utilization. HVDC transmission proves beneficial in facilitating the transfer of renewable energy from resource-rich regions to areas with high electricity demand, but effective load flow analysis is essential to optimize these transfers and maximize the use of clean energy sources. Furthermore, with the expansion of power grids and the interconnectedness of regional networks, system stability and reliability

become paramount concerns. The AC-DC load flow analysis plays a critical role in evaluating the impact of HVDC converter controls and power modulation on overall system stability, ensuring secure operation under various operating conditions.

The integration of renewable energy sources and HVDC transmission has significantly impacted power system analysis and management. As modern power grids evolve into hybrid AC-DC systems, researchers have been investigating various aspects of AC-DC load flow analysis to address the challenges arising from this integration [1]. This comprehensive review explores the integration of HVDC transmission into AC load flow analysis. The authors examine various methodologies and algorithms proposed to accurately model HVDC converters, control strategies, and commutation processes. The paper discusses the impact of HVDC on power flow patterns, voltage profiles, and system stability in hybrid AC-DC networks [2]. This systematic review focuses on load flow optimization techniques in hybrid AC-DC power systems. The authors survey various optimization algorithms, such as Newton-Raphson, Gauss-Seidel, and evolutionary algorithms. The paper emphasizes the importance of load flow optimization in minimizing transmission losses, enhancing energy efficiency, and achieving optimal power flow in integrated AC-DC grids [3]. This research investigates the impact of renewable energy sources, such as solar and wind power, on AC-DC load flow analysis. The authors address the challenges posed by the intermittent nature of renewables and their integration into hybrid power systems. The study discusses the use of energy storage systems and advanced control strategies to ensure grid stability and efficient power flow [4]. This paper reviews the role of Flexible AC Transmission System (FACTS) devices, such as Static Var Compensators (SVC) and Thyristor-Controlled Series Compensators (TCSC), in AC-DC load flow analysis. The authors examine different control strategies employed by FACTS devices to regulate voltage, improve power quality, and enhance system stability. The research highlights the importance of coordinated control between FACTS devices and HVDC converters for optimal performance in hybrid AC-DC networks [5]. This research paper provides a comprehensive review of the challenges and recent advances in AC-DC load flow analysis of power systems. It discusses the complexities arising from the integration of HVDC transmission, FACTS devices, and renewable energy sources. The study presents innovative solutions and state-of-the-art techniques to improve load flow analysis accuracy and efficiency in hybrid AC-DC grids [6]. Focusing on harmonic analysis, this study explores the impact of SVC and TCSC integration in AC-DC load flow analysis. The authors investigate harmonic generation and mitigation challenges introduced by these FACTS devices. The paper presents harmonic modeling techniques to assess power quality and equipment performance, emphasizing the importance of harmonic studies for reliable and efficient operation in hybrid AC-DC power systems [7]. This study explores the coordinated control of HVDC and FACTS devices in AC-DC load flow analysis for optimal power flow management. The authors propose control strategies to enhance power system stability, voltage regulation, and minimize transmission losses. The paper highlights the benefits of synergistic control between HVDC converters and FACTS devices for improving the overall performance of hybrid AC-DC grids [8]. This research investigates real-time AC-DC load flow analysis considering large-scale renewable energy integration. The study addresses the challenges of intermittent renewables and their impact on power system stability. It presents real-time simulation techniques to assess grid performance, contingency analysis, and dynamic response in hybrid AC-DC power systems with significant renewable energy penetration [9]. AC-DC load flow analysis remains crucial for understanding and optimizing hybrid power systems. Efforts are continuously being made to improve modeling

techniques, convergence algorithms, and data availability to enhance the reliability and applicability of AC-DC load flow studies. In this paper, a methodology and mathematical modeling to model AC-DC load flow problem along with necessary graphical and numerical results are presented.

II. MATHEMATICAL MODELING OF AC-DC LOAD FLOW PROBLEM

A concise mathematical modeling of AC-DC load flow with equations:

1. **AC Network Equations:**
   - Nodal Voltage Equations (AC):
     For each AC bus i, the nodal voltage is represented as:

     $$V_{iAC} = |V_{iAC}| \angle \delta_{iAC}$$

     Active Power (P) and Reactive Power (Q) Equations (AC):
   - The active and reactive power at AC bus i are given by:

$$P_{iAC} = |V_{iAC}| \sum_{j=1}^{n} |V_{jAC}| (G_{ij}\cos(\delta_{iAC} - \delta_{jAC}) + B_{ij}\sin(\delta_{iAC} - \delta_{jAC}))$$
$$Q_{iAC} = |V_{iAC}| \sum_{j=1}^{n} |V_{jAC}| (G_{ij}\sin(\delta_{iAC} - \delta_{jAC}) - B_{ij}\cos(\delta_{iAC} - \delta_{jAC}))$$

where: |V_i^{AC}|: Voltage magnitude at bus i in the AC network. δiAC: Phase angle at bus i in the AC network. n: Total number of buses in the AC network. G_{ij}: Conductance between buses i and j in the AC network. B_{ij}: Susceptance between buses i and j in the AC network.

2. **DC Network Equations:**
   - Nodal Voltage Equations (DC):
     For each DC bus i, the nodal voltage is represented as:

$$V_{iDC} = V_{iDC}$$

   - Active Power (P) Equations (DC):
     The active power at DC bus i is given by:

$$P_{iDC} = \sum_{j=1}^{m} V_{iDC} V_{jDC} G_{ij}$$

   - DC Power Flow Equations:
     The power flow between two DC buses i and j is given by:

$$P_{ijDC} = (V_{iDC} - V_{jDC}) G_{ij}$$

where: ViDC: Voltage magnitude at bus i in the DC network. m: Total number of buses in the DC network. G_{ij}: Conductance between buses i and j in the DC network.

The AC and DC load flow equations are typically solved iteratively to find the steady-state operating conditions of the hybrid AC-DC power system. This process involves initializing the voltage magnitudes and phase angles, and then iteratively updating these values until the system reaches a converged solution. Various numerical methods, such as the Gauss-Seidel or Newton-Raphson method, can be used for solving these equations efficiently.

1. **Evaluation of Derivatives:** Below are provided the elements for both the diagonal and off-diagonal components of each sub-matrix within the Jacobian matrix:

A sub matrix

$$J_1 = \frac{\partial P}{\partial \delta}$$

$$\frac{\partial P_i}{\partial \delta_i} = -Q_{i,cal}(|V|, \delta) - B_{ii}|V_i|^2$$

$$\frac{\partial P_i}{\partial \delta_j} = -|V_j V_i Y_{ij}| \sin(\theta_{ij} + \delta_j - \delta_i)$$

B sub matrix

$$J_4 = |V| \frac{\partial P}{\partial |V|}$$

$$|V_i| \frac{\partial Q_i}{\partial |V_i|} = -\frac{\partial P_i}{\partial \delta_i} - 2B_{ii}|V_i|^2$$

$$|V_j| \frac{\partial Q_i}{\partial |V_j|} = +\frac{\partial P_i}{\partial \delta_j}$$

$$|V_i| \frac{\partial Q_i}{\partial |V_i|} = -\frac{\partial P_i}{\partial \delta_j} - 2B_{ii}|V_i|^2 + Q_{i,cal}(|V|, U_{dc})$$

$$|V_j| \frac{\partial Q_i}{\partial |V_j|} = +\frac{\partial P_i}{\partial \delta_j}$$

C sub matrix

$$J_3 = \frac{\partial Q}{\partial \delta}$$

$$\frac{\partial Q_i}{\partial \delta_i} = P_{i,cal}(|V|, \delta) - G_{ii}|V_i|^2$$

$$\frac{\partial Q_i}{\partial \delta_j} = -|V_j V_i Y_{ij}| \cos(\theta_{ij} + \delta_j - \delta_i)$$

D sub matrix

$$J_2 = |V| \frac{\partial P}{\partial |V|}$$

$$|V_i| \frac{\partial P_i}{\partial |V_i|} = \frac{\partial Q_i}{\partial \delta_i} + 2G_{ii}|V_i|^2$$

$$|V_j| \frac{\partial P_i}{\partial |V_j|} = |V_j V_i Y_{ij}| \cos(\theta_{ij} + \delta_j - \delta_i) = -\frac{\partial Q_i}{\partial \delta_i}$$

$$|V_j| \frac{\partial P_i}{\partial |V_j|} = |V_j V_i Y_{ij}| \cos(\theta_{ij} + \delta_j - \delta_i) = -\frac{\partial Q_i}{\partial \delta_i}$$

$$|V_i| \frac{\partial P_i}{\partial |V_i|} = -\frac{\partial Q_i}{\partial \delta_i} - 2G_{ii}|V_i|^2 + P_{i,cal}(|V|, U_{dc})$$

III. MODELING OF SERIES FACTS CONTROLLERS

Series FACTS (Flexible AC Transmission Systems) controllers are power electronics-based devices used to control and enhance the transmission of electrical power in AC

(alternating current) systems. They are installed in series with the transmission line and can regulate the line impedance and voltage, leading to an improvement in power transfer capability and system stability. These devices play a crucial role in modern power systems by providing dynamic control and flexibility, especially in dealing with transmission congestion and stability issues. It is important to note that while series FACTS controllers offer significant benefits, their deployment and operation require careful consideration and coordination to avoid any potential issues related to system protection, stability, and harmonics. Thus, comprehensive system studies and simulations are conducted before implementing series FACTS devices in the power grid.

1. **Operating principle of TCSC:** The Thyristor-Controlled Series Capacitor (TCSC) is categorized as a series FACTS controller utilized within power systems to augment control and stability of transmission lines. Its operating principle involves the control of the line reactance using thyristor switches in a series capacitor configuration shown in Fig.1.

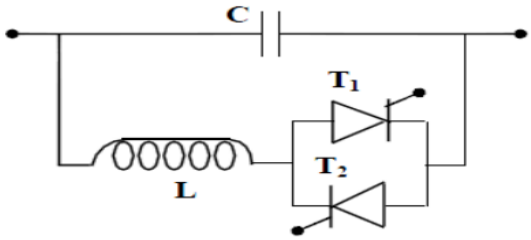

Figure 1: Model of TCSC

In order to assess the impact of this equipment, it is necessary to integrate the TCSC into the existing system. To achieve this, the power injection model for the TCSC is outlined as follows:

Consider a simplified transmission system represented by π-equivalent parameters, where a linkage exists between bus-s and bus-r. The flow of real and reactive power from bus-s to bus-r can be mathematically expressed as follows:

$$P_{sr} = V_s^2 G_{sr} - V_s V_r [G_{sr}\text{Cos}(\delta_{sr}) + B_{sr}\text{Sin}(\delta_{sr})]$$
$$Q_{sr} = -V_s^2 (B_{sr} + B_{sh}) - V_s V_r [G_{sr}\text{Sin}(\delta_{sr}) - B_{sr}\text{Cos}(\delta_{sr})]$$

Where $\delta_{sr} = \delta_s - \delta_r = -\delta_{rs}$

The flow of real and reactive power from bus-r to bus-s is.

$$P_{rs} = V_r^2 G_{sr} - V_s V_r [G_{sr}\text{Cos}(\delta_{sr}) - B_{sr}\text{Sin}(\delta_{sr})]$$
$$Q_{rs} = -V_r^2 (B_{sr} + B_{sh}) + V_s V_r [G_{sr}\text{Sin}(\delta_{sr}) + B_{sr}\text{Cos}(\delta_{sr})]$$

2. **Power Injection Model of TCSC:** In Figure 2, we observe a transmission line configuration featuring a Thyristor-Controlled Series Capacitor (TCSC) linked between bus-s and bus-r. During stable operating conditions, the TCSC is characterized as a fixed reactance. Within the power flow equations, the manipulable reactance serves as the immediate control parameter.

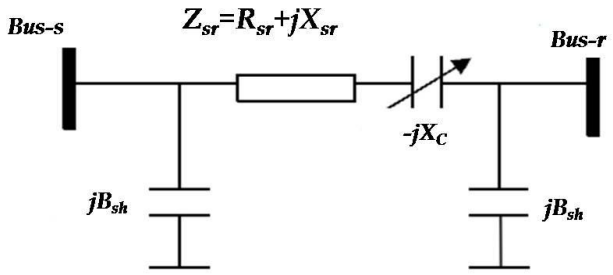

Figure 2: Transmission line with TCSC

Upon integration of the TCSC within the line configuration, modifications will be made to the line parameters. The adjusted line reactance can be expressed as follows:

$$X_{\text{srnew}} = X_{\text{sr}} - X_C$$

Consequently, the recalibrated line admittance between buses "s" and "r" can be deduced through the ensuing derivation:

$$Y'_{\text{sr}} = \frac{1}{Z'_{\text{sr}}} = \frac{1}{R_{\text{sr}}+j(X_{\text{sr}}-X_C)}\ ;\ Y'_{\text{sr}} = G'_{\text{sr}} + \text{jB}'_{\text{sr}} = \frac{R_{\text{sr}}-j(X_{\text{sr}}-X_C)}{R_{\text{sr}}^2+(X_{\text{sr}}-X_C)^2}$$

$$G'_{\text{sr}} = \frac{R_{\text{sr}}}{R_{\text{sr}}^2+(X_{\text{sr}}-X_C)^2} \qquad B'_{\text{sr}} = -\frac{(X_{\text{sr}}-X_C)}{R_{\text{sr}}^2+(X_{\text{sr}}-X_C)^2}$$

The updated real and reactive power transfers between bus-s and bus-r, as well as between bus-r and bus-s, for a transmission line with integrated series impedance and series reactance, are presented below:

$$P_{\text{sr}}^{\text{TCSC}} = V_s^2 G'_{\text{sr}} - V_s V_r\left(G'_{\text{sr}}\text{Cos}(\delta_{\text{sr}}) + B'_{\text{sr}}\text{Sin}(\delta_{\text{sr}})\right)$$
$$Q_{\text{sr}}^{\text{TCSC}} = -V_s^2(B'_{\text{sr}} + B_{\text{sh}}) - V_s V_r\left(G'_{\text{sr}}\text{Sin}(\delta_{\text{sr}}) - B'_{\text{sr}}\text{Cos}(\delta_{\text{sr}})\right)$$
$$P_{\text{rs}}^{\text{TCSC}} = V_r^2 G'_{\text{sr}} - V_s V_r\left(G'_{\text{sr}}\text{Cos}(\delta_{\text{sr}}) - B'_{\text{sr}}\text{Sin}(\delta_{\text{sr}})\right)$$
$$Q_{\text{rs}}^{\text{TCSC}} = -V_r^2(B'_{\text{sr}} + B_{\text{sh}}) + V_s V_r\left(G'_{\text{sr}}\text{Sin}(\delta_{\text{sr}}) + B'_{\text{sr}}\text{Cos}(\delta_{\text{sr}})\right)$$

The power loss in the transmission line equipped with TCSC can be expressed as follows:

$$P_{\text{Loss}} = P_{\text{sr}}^{\text{TCSC}} + P_{\text{rs}}^{\text{TCSC}} = G'_{\text{sr}}(V_s^2 + V_r^2) - 2\text{V}_s V_r G'_{\text{sr}}\text{Cos}(\delta_{\text{sr}})$$
$$Q_{\text{Loss}} = Q_{\text{sr}}^{\text{TCSC}} + Q_{\text{rs}}^{\text{TCSC}} = -(V_s^2 + V_r^2)(B'_{\text{sr}} + B_{\text{sh}}) + 2\text{V}_s V_r B'_{\text{sr}}\text{Cos}(\delta_{\text{sr}})$$

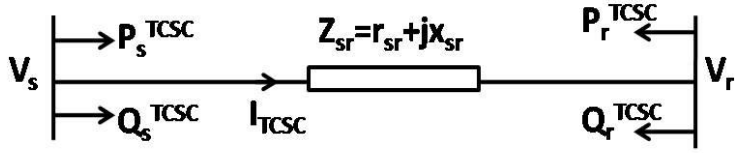

Figure 3: Power injection model of TCSC

Because of the inclusion of TCSC, alterations in line flow can be envisioned through an analogous line configuration without TCSC. This is accompanied by power injections at both the originating and receiving terminals of the line, as illustrated in

Figure 3. The mathematical representation of the active and reactive power injections at bus-s and bus-r is as follows:

$$P_s^{\mathrm{TCSC}} = P_{\mathrm{sr}} - P_{\mathrm{sr}}^{\mathrm{TCSC}} = V_s^2 \Delta \mathrm{G}_{\mathrm{sr}} - V_s V_r [\Delta \mathrm{G}_{\mathrm{sr}} \mathrm{Cos}(\delta_{\mathrm{sr}}) + \Delta \mathrm{B}_{\mathrm{sr}} \mathrm{Sin}(\delta_{\mathrm{sr}})]$$
$$P_r^{\mathrm{TCSC}} = P_{\mathrm{rs}} - P_{\mathrm{rs}}^{\mathrm{TCSC}} = V_s^2 \Delta \mathrm{G}_{\mathrm{sr}} - V_s V_r [\Delta \mathrm{G}_{\mathrm{sr}} \mathrm{Cos}(\delta_{\mathrm{sr}}) - \Delta \mathrm{B}_{\mathrm{sr}} \mathrm{Sin}(\delta_{\mathrm{sr}})]$$
$$Q_s^{\mathrm{TCSC}} = Q_{\mathrm{sr}} - Q_{\mathrm{sr}}^{\mathrm{TCSC}} = -V_s^2 \Delta \mathrm{B}_{\mathrm{sr}} - V_s V_r [\Delta \mathrm{G}_{\mathrm{sr}} \mathrm{Sin}(\delta_{\mathrm{sr}}) - \Delta \mathrm{B}_{\mathrm{sr}} \mathrm{Cos}(\delta_{\mathrm{sr}})]$$
$$Q_r^{\mathrm{TCSC}} = Q_{\mathrm{rs}} - Q_{\mathrm{rs}}^{\mathrm{TCSC}} = -V_r^2 \Delta \mathrm{B}_{\mathrm{sr}} + V_s V_r [\Delta \mathrm{G}_{\mathrm{sr}} \mathrm{Sin}(\delta_{\mathrm{sr}}) + \Delta \mathrm{B}_{\mathrm{sr}} \mathrm{Cos}(\delta_{\mathrm{sr}})]$$

Where

$\Delta \mathrm{G}_{\mathrm{sr}} = \frac{X_C R_{\mathrm{sr}} (X_C - 2\mathrm{X}_{\mathrm{sr}})}{(R_{\mathrm{sr}}^2 + X_{\mathrm{sr}}^2)(R_{\mathrm{sr}}^2 + (X_{\mathrm{sr}} - X_C)^2)}$, $\Delta \mathrm{B}_{\mathrm{sr}} = \frac{-X_C (R_{\mathrm{sr}}^2 - X_{\mathrm{sr}}^2 + X_C X_{\mathrm{sr}})}{(R_{\mathrm{sr}}^2 + X_{\mathrm{sr}}^2)(R_{\mathrm{sr}}^2 + (X_{\mathrm{sr}} - X_C)^2)}$

The TCSC device has been modeled using a power injection approach, incorporating the TCSC control variable. Consequently, it is feasible to compute the complex power injected at bus-s and bus-r, respectively.

$S_s^{\mathrm{TCSC}} = P_s^{\mathrm{TCSC}} + jQ_s^{\mathrm{TCSC}}$, $S_r^{\mathrm{TCSC}} = P_r^{\mathrm{TCSC}} + jQ_r^{\mathrm{TCSC}}$

Subsequently, the new power flow equations can be formulated using the following relationship:

$$\begin{bmatrix} \Delta \mathrm{P} \\ \Delta \mathrm{Q} \end{bmatrix} = \begin{bmatrix} H_{\mathrm{new}} & M_{\mathrm{new}} \\ N_{\mathrm{new}} & L_{\mathrm{new}} \end{bmatrix} \cdot \begin{bmatrix} \Delta \delta \\ \frac{\Delta \mathrm{V}}{V} \end{bmatrix}$$

Where, new mismatch vectors are

$$\Delta \mathrm{P}_i = P_i^{\mathrm{spec}} + P_i^{\mathrm{TCSC}} - P_i^{\mathrm{Calc}}; \forall i = \mathrm{s,r}$$
$$\Delta \mathrm{Q}_i = Q_i^{\mathrm{spec}} + Q_i^{\mathrm{TCSC}} - Q_i^{\mathrm{Calc}}; \forall i = \mathrm{s,r}$$

P_i^{spec} and Q_i^{spec} These are the conventional specified real and reactive powers, P_i^{TCSC} and Q_i^{TCSC} These are the power injections associated with TCSC devices. $P_i^{\mathrm{calc}}$and Q_i^{calc} The power injections linked to TCSC devices are calculated using the power flow equations. Subsequently, the modified Jacobian matrix, resulting from the power injections of TCSC, can be obtained as follows:

$H_{\mathrm{new}} = H + \frac{\partial {P_i}^{\mathrm{TCSC}}}{\partial \delta} \forall i = \mathrm{s,r}$; $M_{\mathrm{new}} = M + \frac{\partial {P_i}^{\mathrm{TCSC}}}{\partial V} V \forall i = \mathrm{s,r}$

$N_{\mathrm{new}} = N + \frac{\partial {Q_i}^{\mathrm{TCSC}}}{\partial \delta} \forall i = \mathrm{s,r}$; $L_{\mathrm{new}} = L + \frac{\partial {Q_i}^{\mathrm{TCSC}}}{\partial V} V \forall i = \mathrm{s,r}$

H, M, N and L are the classic sub-Jacobian matrices.

IV. MODELING OF SHUNT FACTS CONTROLLERS

As per the IEEE definition, a Static Var Compensator (SVC) is a shunt-connected device responsible for generating or absorbing reactive power. Its output can be precisely adjusted to exchange capacitive or inductive current, effectively regulating specific parameters within the electrical power system, often focusing on maintaining bus voltage.

SVCs find extensive application in power systems to elevate voltage levels, thereby enhancing overall system stability. By offering reactive power support, SVCs play a vital role in ensuring voltage remains within acceptable limits and mitigating voltage fluctuations, thereby contributing to a dependable and consistent power supply.

1. **Modeling of SVC:** In practical scenarios, the Static Var Compensator (SVC) can be conceptualized as a variable reactance with constraints on firing angles or reactance values. To establish the nonlinear power equations for the SVC, the equivalent circuit depicted in Figure 4 is utilized. As indicated in Figure 4, the SVC's current consumption is computed using the subsequent equation:

$$I_{\mathrm{SVC}} = \mathrm{j}B_{\mathrm{SVC}}V_i$$

The reactive power drawn by the SVC, which also signifies the reactive power injected at bus-i, can be calculated as follows:

$$Q_{\mathrm{SVC}} = Q_i = -V_i^2 B_{\mathrm{SVC}}$$

The SVC is designed as a collection of three-phase static capacitors and/or inductors. Under high load conditions, when positive reactive power (VAr) is necessitated, capacitor banks are engaged; conversely, inductor banks are employed for negative VAr requirements. In this thesis, the SVC is represented as an ideal source of reactive power injection at bus-i, as illustrated in Figure 4.

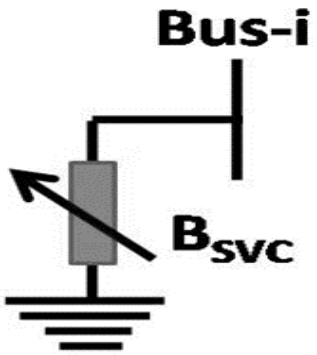

Figure 4: Power injection model of SVC

V. POWER SYSTEM PERFORMANCE PARAMETERS

This section provides an explanation of various electrical parameters within a power system and their influence on the overall system parameters. It delves into how changes in these parameters can impact the performance and behavior of the power system.

1. **Generation Fuel Cost:** The primary goal of a power generation system is to fulfill the demand while minimizing fuel costs. The total fuel cost function can be mathematically expressed as follows:

$$\text{FC} = \sum_{i=1}^{\text{NG}} C_i(P_{\text{Gi}})\ \$/\text{h}$$

The total generation fuel cost, represented by 'FC,' is obtained by summing up the individual fuel cost functions for each generating unit 'Ci(PGi).' In this equation, 'PGi' represents the power generated by the ith unit, and 'NG' denotes the total number of generating units.

The objective function is formulated as a quadratic fuel cost function. The quadratic fuel cost of a thermal generating unit can be represented using a second-order polynomial function in the following manner:

$$C_i(P_{\text{Gi}}) = a_i P_{\text{Gi}}^2 + b_i P_{\text{Gi}} + c_i \$/\text{hr}$$

where, ai, bi, and ci are the fuel-cost coefficients of the ith unit,

2. **Emission objective:** The release of gases within the boiler is distinguished by the combination of several emitted gases, including NO2, SO2, thermal emissions, and others. The amount of emitted gases correlates with the generator's output and is illustrated by the following representation:

$$A_2 = \min\left[E\left(P_{G_i}\right)\right] = \sum_{i=1}^{\text{NG}} e_i\ (\text{ton/h})$$

where e_i is the emission of the i^{th}generator

The emission curve is represented in quadratic function as

$e_i = \alpha_i + \beta_i P_{\text{Gi}} + \gamma_i P_{\text{Gi}}^2 + \xi_i \exp(\lambda_i P_{\text{Gi}})$ (ton/h)

Where $\alpha_i, \beta_i, \gamma_i, \xi_iand\lambda_i$ are the emission coefficients of the i^{th}generator

3. **Total Power Losses:** The objective function employed for calculating the total power loss (TPL) encompasses the power transmission through a line, ascertainable through the power flow solution. The expression for power loss is articulated as follows:

$$A_3 = \min(\text{TPL}) = \sum_{i=1}^{\text{nl}} P_{\text{Loss}_i}$$

Where $P_{Loss_i}$is the real power loss in i^{th}line

4. **Transmission Line Voltage Regulation:** Voltage regulation for a transmission line is described as the percentage proportion between the disparity of sending and receiving end voltages, relative to the receiving end voltage. This evaluation is conducted under the circumstances of both no load and full load conditions.

The voltage regulation (%VR) can be expressed mathematically as:

$$\%\text{VR} = \frac{V_S - V_R}{V_R} \times 100$$

Here, Vs represents the sending end voltage per phase, and VR is the receiving end voltage per phase.

The sending end voltage (Vs) is calculated using the following formula:

$$V_S = \sqrt{(V_R \mathrm{Cos}\theta_R + \mathrm{IR})^2 + (V_R \mathrm{Sin}\theta_R + \mathrm{IX}_L)^2}$$

Where XL is the reactance per phase, R is the resistance per phase, θR is the receiving end power factor.

5. **Transmission Efficiency:** Transmission efficiency is quantified as the percentage relationship between the power received at the endpoint (PR) and the power dispatched from the source (PS) within a power transmission setup. It elucidates the effectiveness of power conveyance from the initial point to the terminal of the transmission line. This efficiency parameter is denoted as a percentage.

$$\%\eta\mathrm{T} = \frac{P_R}{P_S} \times 100$$

6. **Corona loss:** Whenever corona is formed in a power system, energy loss is unavoidable, and it dissipates through various forms, including light, heat, sound, and chemical reactions. When the voltage exceeds the disruptive threshold, the power loss due to corona can be mathematically expressed as follows:

$$P = 241(f + 25)\sqrt{\frac{r}{d}}\left[V_0 - 21.1\mathrm{K}_i \mathrm{r}\ln\left(\frac{d}{r}\right)\right]^2 \times 10^{-5}\mathrm{kW/km}$$

F=frequency in Hz

VI. RESULTS AND ANALYSIS

The efficiency of the developed methodology is assessed using the IEEE-14 bus test system [Ref]. This system comprises fourteen buses, twenty-one transmission lines, with five generators located at buses 1, 2, 3, 6, and 8, one shunt compensator at bus-9, and three tap-changing transformers installed in lines 8 (between buses 4 and 7), 9 (between buses 4 and 9), and 10 (between buses 5 and 6). The total active and reactive power loads are 246.05 MW and 69.825 MVAr, respectively. To formulate the AC-DC network, the 13th transmission line, which connects buses 7 and 9, is considered as the DC link. In this line, the rectifier is connected at bus-7, and the inverter is connected at bus-9.

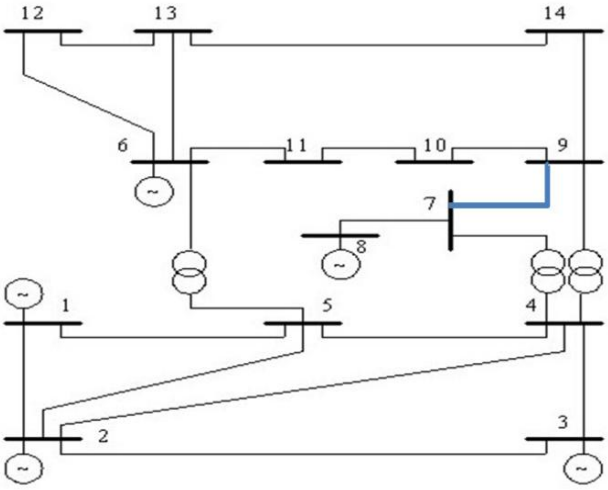

Single line diagram of IEEE-14 bus system with DC link

The entire analysis is performed for the following modules:
Module-1: Identifying the effectiveness of AC-DC network over conventional AC network.
Module-2: Analyzing the effect of converter parameters such as rectifier delay angle (α) and inverter extinction angle (β) on system parameters. For this, these angles are varied from 0 deg to 360 deg in steps of 20 deg.
Module-3: Analyzing the effect of AC-DC load flow on various power system parameters.
Module-4: Analyzing the effect of FACTs controllers such as SVC and TCSC on various power system parameters when compared to without device.

Module-1

In this module, both NR load flow problem is solved for the AC network and AC-DC networks. To identify the effect of DC link on system parameters, the rectifier delay angle (α) and inverter extinction angle (β) are assumed to be 60 deg and 220 deg respectively. The obtained load flow results for the voltage magnitude and voltage angles are tabulated in Table.1. From this, it is identified that, the voltage magnitude at bus-7 is enhanced and bus-9 is decreased. This is due to operation of $\alpha < 180$ deg and $\beta > 180$ deg. The variation of voltage magnitudes and voltage angles are shown in Figs.5 and 6.

Table 1: Voltages with AC-DC NR load flow method for IEEE-14 bus system

Bus No	VM, p.u.		VA, deg	
	AC NR	AC-DC NR	AC NR	AC-DC NR
1	1.06	1.06	0	0
2	1.045	1.045	-2.312	-2.243
3	1.011	1.012	-6.012	-5.866
4	1.024	1.024	-5.945	-5.844
5	1.026	1.026	-4.98	-4.93
6	1.07	1.07	-8.048	-8.244
7	1.064	1.065	-7.781	-7.264
8	1.09	1.09	-6.911	-6.395
9	1.057	1.053	-9.299	-9.756

10	1.052	1.049	-9.35	-9.76
11	1.058	1.056	-8.828	-9.131
12	1.056	1.056	-8.898	-9.115
13	1.051	1.051	-9.016	-9.249
14	1.038	1.035	-10.124	-10.487

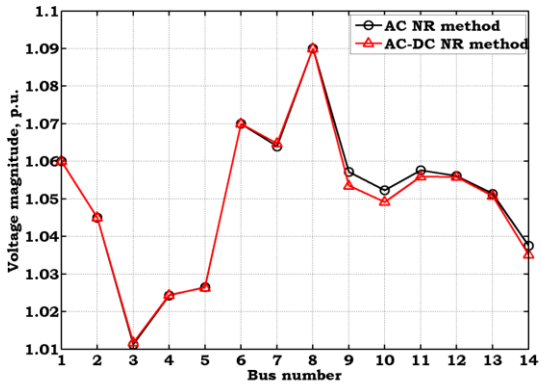

Figure 5: Variation of voltage magnitude with AC-DC NR load flow method for IEEE-14 bus system

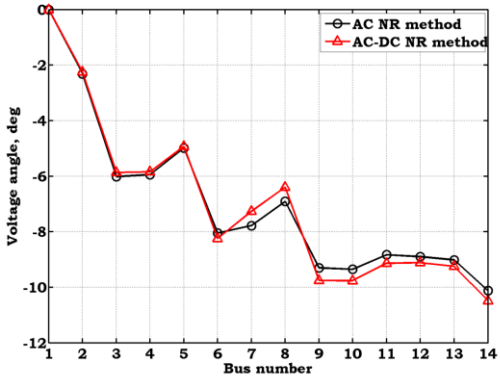

Figure 6: Variation of voltage angle with AC-DC NR load flow method for IEEE-14 bus system

Similarly, the power flow results are tabulated in Table.2. From this result, it is identified that, power flow through DC link is decreased from 27.95 MVA to 23.909 MVA. The variation of power flow is shown in Fig.7.

Table.2 Power flows with AC-DC NR load flow method for IEEE-14 bus system

Line No	Power flow, MVA	
	AC NR	AC-DC NR
1	76.618	74.547
2	44.28	43.896
3	37.687	36.943
4	38.723	38.407

5	29.421	29.636
6	8.871	8.638
7	40.226	38.066
8	18.875	15.72
9	11.759	13.71
10	28.866	30.64
11	9.261	10.513
12	7.934	8.101
13	18.945	19.602
14	18.577	18.19
15	27.95	23.909
16	5.845	5.068
17	8.755	7.993
18	5.536	6.732
19	1.842	2.003
20	6.633	7.429

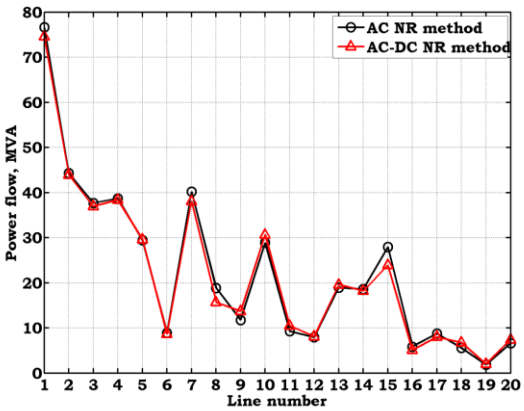

Figure 7: Variation of power flow with AC-DC NR load flow method for IEEE-14 bus system

Furthermore, the results for active and reactive power losses, number of iterations, and time taken for convergence are tabulated in Table 3. The analysis reveals that the total active power losses decrease with the inclusion of the DC link in the AC network. Similarly, the total number of iterations required for convergence is reduced. However, due to the increased computational complexity, the time taken for convergence is extended.

Table 3: Power losses and performance parameters with AC-DC NR load flow method for IEEE-14 bus system

Parameters	AC NR	AC-DC NR
Active power losses, MW	4.635	4.563
Reactive power losses, MVAr	-8.665	-8.441
Number of Iterations	5	4
Time, Sec	0.053	0.097

Module-2

Furthermore, to examine the impact of DC link converters on system performance, the analysis is conducted by varying the rectifier delay angle (α) and inverter extinction angle (β). These angles are systematically changed from 0 degrees to 360 degrees in increments of 20 degrees.

At each angle variation, the minimum and maximum voltage magnitudes at buses, along with their corresponding α and β values, are recorded and presented in Table 4. The analysis reveals that the generator connected at bus-3 is no longer operating as a PV bus due to the rectifier operation at bus-5. Additionally, the maximum voltage difference is observed at bus-3, while the minimum difference is observed at bus-12. A graphical representation of the voltage differences at various buses is illustrated in Fig. 8.

Table.4 Variation of voltage magnitudes with AC-DC NR load flow method for IEEE-14 bus system

Bus No	V_{min} (p.u.)	α (deg)	β (deg)	V_{max} (p.u.)	α (deg)	β (deg)	V_{diff} (p.u.)
1	1.06	0	0	1.06	0	0	0
2	1.045	0	0	1.045	0	0	0
3	1.01	0	80	1.012	60	240	-0.0028
4	1.024	60	80	1.025	0	240	-0.0007
5	1.026	60	80	1.026	0	240	-0.0004
6	1.07	0	0	1.07	0	0	0
7	1.065	60	80	1.065	0	240	-0.0003
8	1.09	0	0	1.09	0	0	0
9	1.053	0	180	1.054	60	20	-0.0003
10	1.049	0	180	1.049	60	20	-0.0002
11	1.056	0	180	1.056	60	20	-0.0001
12	1.056	60	80	1.056	0	240	-2E-05
13	1.051	0	180	1.051	60	20	-4E-05
14	1.035	0	180	1.035	60	20	-0.0002

$$V_{diff}=V_{max}-V_{min}$$

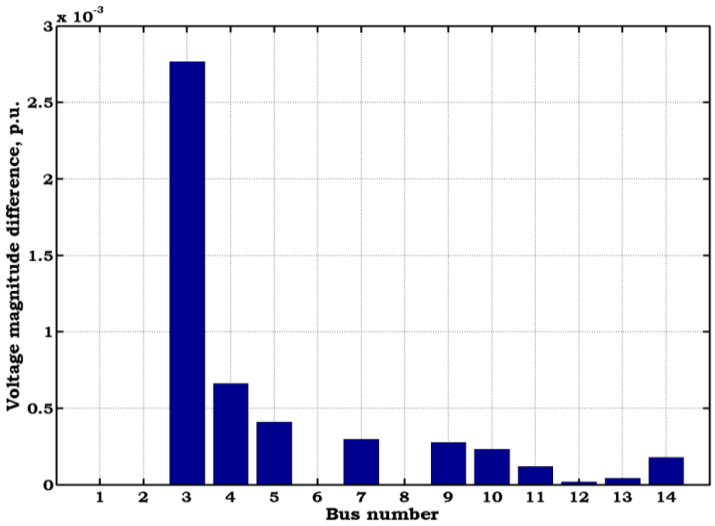

Figure 8: Variation of voltage difference with AC-DC NR load flow method for IEEE-14 bus system

Similarly, for each step of angles variation, the minimum and maximum power flow in transmission lines along with respective α and β values are tabulated in Table.5. From this table, it is observed that, the first transmission line connected to slack has major variation of power flow. As the generation from slack bus is increased to divert the power to the loads. The variation of power flow difference in lines is shown in Fig.9.

Table 5: Variation of power flow with AC-DC NR load flow method for IEEE-14 bus system

Line No	S_{min} (p.u.)	α (deg)	β (deg)	S_{max} (p.u.)	α (deg)	β (deg)	S_{diff} (p.u.)
1	74.537	60	0	78.592	0	60	-4.055
2	43.895	60	0	44.967	0	60	-1.072
3	36.879	0	220	38.34	60	60	-1.461
4	38.262	0	220	38.77	60	60	-0.508
5	29.443	0	220	29.822	60	60	-0.38
6	8.308	60	240	9.444	0	80	-1.136
7	38.06	60	0	39.018	0	160	-0.958
8	15.679	0	140	15.775	60	80	-0.096
9	13.679	0	280	13.711	60	120	-0.032
10	30.605	60	300	30.692	0	140	-0.088
11	10.511	60	120	10.556	0	280	-0.045
12	8.1	60	340	8.107	0	180	-0.007
13	19.6	60	120	19.626	0	180	-0.025
14	18.149	0	240	18.295	60	80	-0.146
15	23.875	0	280	23.909	60	220	-0.034
16	5.027	0	80	5.083	60	240	-0.056
17	7.963	0	180	7.997	60	340	-0.034

18	6.732	60	120	6.772	0	280	-0.04
19	2.003	60	340	2.01	0	180	-0.007
20	7.429	60	120	7.457	0	280	-0.028

$S_{diff}=S_{max}-S_{min}$

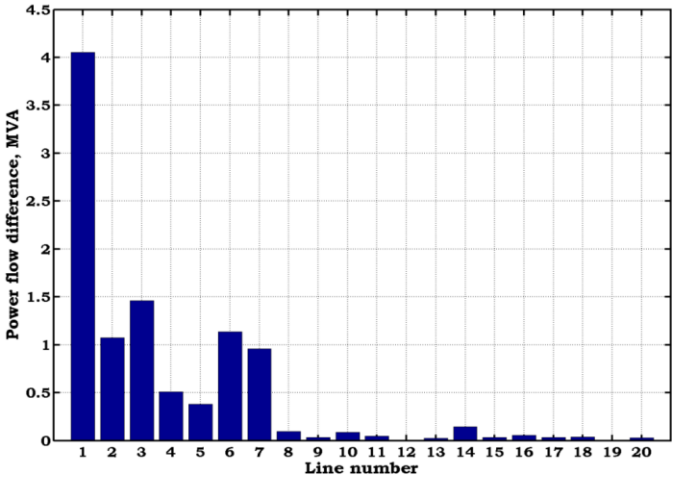

Figure 9: Variation of power flow difference with AC-DC NR load flow method for IEEE-14 bus system

At last, minimum and maximum power losses along with respective α and β values are tabulated in Table.6. From this, it is observed that, there is a power loss difference of 0.222 MW with DC link.

Table 6: Variation of power loss with AC-DC NR load flow method for IEEE-14 bus system

	$Ploss_{min}$ (MW)	**α (deg)**	**β (deg)**	**$Ploss_{max}$ (MW)**	**α (deg)**	**β (deg)**	**$Ploss_{diff}$ (MW)**
P loss, MW	4.562806	60	220	4.78495	0	60	0.222144

Module-3

To extend the benefit of AC-DC transmission for power system performance enhancement, certain power system parameters are considered and the corresponding results are tabulated in Table.7. Due to DC link, the sending and receiving end voltage magnitudes are increased, this in turn decreases the line current, power flows, total generation, generation cost, emission of flue gases and total power losses. Also, voltage regulation is decreased which increases the total transmission efficiency. It is also observed that, in AC-DC system, corona losses are decreased by 62.6053 kW when compared to AC system.

Table 7: Power system parameters with AC-DC NR load flow method for IEEE-14 bus system

S. No	Parameter	AC NR method	AC-DC NR method
1	Sending end voltage magnitude (V_S), p.u.	1.063954	1.064737
2	Receiving end voltage magnitude (V_r), p.u.	1.057153	1.059124
3	Line current (I_{line}), Amps	0.2433-j0.0990	0.2089-j0.0855
4	Active power flow (7-9), MW	27.07624	23.21865
5	Reactive power flow (7-9), MVAr	6.935814	5.705615
6	Apparent power flow (7-9), MVA	27.95046	23.90941
7	Total generation, MW	250.68528	250.61281
8	Generation cost, $/hr	2175.0675	2150.9896
9	Emission, ton/hr	10.639068	10.366526
10	Total power losses, MW	4.6352826	4.5628056
11	Voltage regulation of line (%)	47.5161	38.9745
12	Transmission efficiency	82.5830	82.8166
13	Corona loss (kW/km)	94.0826	31.4773

Module-4

To evaluate the influence of FACTS controllers on system performance, two types of controllers, the Static VAr Compensator (SVC) as a shunt controller and the Thyristor-Controlled Series Compensator (TCSC) as a series controller, are taken into account.

To determine the optimal placement of the SVC, a bus with low voltage is identified after conducting the AC-DC load flow analysis (as shown in Table 1). Bus-14 is selected as the ideal location for the SVC installation, as it lacks sufficient nearby generator support. The SVC is sized at 50 MVAr.

Similarly, for the series controller (TCSC), a line with a high power flow margin, which indicates the difference between rated capacity and actual power flow, is chosen. In this case, line-6, connecting buses 3 and 4, is considered the most suitable location. The TCSC device's size is set at 80% of the transmission line reactance (0.8 * Xline = 0.034206).

Upon conducting the AC-DC load flow analysis with SVC and TCSC individually, the results for power system parameters are tabulated in Table 8. The analysis clearly demonstrates that the series and shunt compensations influence the power system parameters according to the nature of their compensation.

Table 8: Power system parameters with SVC and TCSC for IEEE-14 bus system

S. No	Parameter	Without device	With SVC	With TCSC
1	Sending end voltage magnitude (V_S), p.u.	1.064737	1.085152	1.064074
2	Receiving end voltage magnitude (V_r), p.u.	1.059124	1.106271	1.052851

3	Line current (I_{line}), Amps	0.2089-j0.0855	0.2313+j0.0662	0.2085-j0.0855
4	Active power flow (7-9), MW	23.21865	23.94129	23.17092
5	Reactive power flow (7-9), MVAr	5.705615	-10.411	6.190107
6	Apparent power flow (7-9), MVA	23.90941	26.10697	23.98351
7	Total generation, MW	250.61281	251.79422	250.66277
8	Generation cost, $/hr	2150.9896	2177.4353	2155.329
9	Emission, ton/hr	10.366526	11.705576	10.413689
10	Total power losses, MW	4.5628056	5.7442168	4.6127721
11	Voltage regulation of line (%)	38.9745	45.9981	34.4679
12	Transmission efficiency	82.8166	87.2366	82.8055
13	Corona loss (kW/km)	31.4773	34.3264	31.1075

VII. CONCLUSIONS

After conducting a thorough literature review, it has been observed that power transfer through a DC link leads to improved system performance compared to conventional AC transmission. To validate this observation, a novel load flow approach for AC-DC systems has been developed. This approach incorporates the sending end rectifier and receiving end inverters in a manner that accounts for the effects of DC transmission in the AC load flow problem. The project presents a comprehensive mathematical formulation to solve the AC-DC load flow problem, along with the integration of the load flow procedure. The analysis indicates that the use of DC transmission enhances overall system performance, resulting in improved voltage profiles and reduced total losses. Furthermore, the study investigates the impact of rectifier delay angle and inverter extinction angles on power system parameters such as voltage magnitude, voltage angle, power flow, and total system losses. The analysis reveals significant variations in the voltage profile near the buses where the DC link is connected. Moreover, the project explores the influence of FACTs controllers on AC-DC system performance in terms of power losses, generation cost, emission levels, voltage regulation, transmission efficiency, and corona losses. The findings demonstrate a notable enhancement in system performance when FACTs controllers are employed in the AC-DC power system compared to the AC power system.

REFERENCES

[1] W. Xi-Fan, S. Yonghua and I. Malcolm, Modern Power Systems Analysis, lSBN 978- 0-387-72852-0, 2009.
[2] G. John and S. William, Power System Analysis, Mcgraw-Hill: lSBN 0-07-061293-5, 1994.
[3] Glenn W. Stagg, Ahmed H. El-Abiad, Computer Methods in Power Systems, Mcgraw-Hill, 1968.
[4] H. E. Brown, G. K. Carter, H. H. Happ and C. E. Person, "Power Flow. Solution By Impedance Matrix Method," IEEE Trans. Power Apparatus and System, April 1963.
[5] Robert G. Andretich, Homxier E. Brown, Harvey H. Happ and Conrad E. Person, "The Piecewise Solution of The Impedance Matrix Load Flow," IEEE Transactions on Power Apparatus And Systems, October 1968,Vol. PAS-87, No. 10, pp.1877-1882.
[6] William F. Tinney and Clifford E. Hart, "Power Flow Solution By Newton's Method," IEEE Transactions On Power Apparatus And Systems, Nov. 1967.
[7] Stott. B. and Alasc. O., "Fast Decoupled Load Flow," IEEE Transactions On Power Apparatus And Systems, PAS-93, pp.859-869, 1974.
[8] J. W. Allen and F. W. Bruce, power Generation, Operation, And Control, Wiley, ISBN:978-0471586999, 1996.

[9] P. S. R. Murty, Operation And Control In Power Systems, Taylor And Francis: ISBN: 9780415665650, 2011.
[10] T. Nguyen, "Neural Network Load-Flow," IEEE Proceedings of Generation Transmission Distribution, Vol. 142, No. 1, Jan. 1995, pp. 51-58.

